Unexpected Rise in Nuclear Collectivity from Short-Range Physics

Unexpected Rise in Nuclear Collectivity from Short-Range Physics

Kevin S. Becker,[1] Kristina D. Launey,[1] Andreas Ekström,[2] Tomáš Dytrych,[1,3] Daniel Langr,[4] Grigor H. Sargsyan,[5] and Jerry P. Draayer[1]

[1]*Department of Physics and Astronomy, Louisiana State University, Baton Rouge, Louisiana 70803, USA*
[2]*Department of Physics, Chalmers University of Technology, SE-412 96 Göteborg, Sweden*
[3]*Nuclear Physics Institute of the Czech Academy of Sciences, 250 68 Řež, Czech Republic*
[4]*Department of Computer Systems, Faculty of Information Technology, Czech Technical University in Prague, Prague 16000, Czech Republic*
[5]*Facility for Rare Isotope Beams, Michigan State University, East Lansing, Michigan 48824, USA*

(Received 12 March 2025; accepted 9 October 2025; published 13 January 2026)

We discover a surprising relation between the collective motion of nucleons within atomic nuclei, traditionally understood to be driven by long-range correlations, and short-range nucleon-nucleon interactions. Specifically, we find that quadrupole collectivity in low-lying states of ^{6}Li and ^{12}C, calculated with state-of-the-art *ab initio* techniques, is significantly influenced by two opposing S-wave contact couplings that subtly alter the surface oscillations of one largely deformed nuclear shape, without changing that shape's overall contribution within the nucleus. The results offer new insights into the nature of emergent nuclear collectivity and its link to the underlying nucleon-nucleon interaction at short distances.

DOI: 10.1103/c3st-tp13

While the emergence of dominant collective shapes in atomic nuclei from elementary particle considerations has been recently shown in large-scale *ab initio* calculations [1], how exactly the underlying physics of quarks and gluons imparts collectivity remains elusive. Nuclear collectivity is historically understood to be driven by long-range correlations that deform the nucleus; deformed nuclei can rotate, which involves all particles in the system in a correlated motion [2]. Every nucleus can take on several shapes, typically one or two [1], and the deformation of each nuclear shape is often inferred from its equilibrium "static" deformation, whereas the "snapshots" of the shape's surface dynamics are called dynamical deformation (Fig. 1). The extent of collectivity is informed by electric quadrupole moments Q_2, or equally, reduced transition strengths $B(E2)$, which increase with larger deformation [3]. The prevalence of large deformation in most nuclei, even those with a practically spherical ground state but with nearby well-deformed excited states [4], is now evident from the vast body of experimental data (see the reviews [5,6] and references therein). Furthermore, recent measurements of $B(E2)$ strengths have achieved such precision that they can now test microscopic approaches and the underlying inter-nucleon forces they adopt (e.g., [7,8]).

Yet, with no available nuclear force expressed directly in quark and gluon degrees of freedom, it remains unclear which parts of such fundamental interactions are responsible for the universal preference of large deformation, and are capable of substantially influencing collectivity. Fortunately, some insight emerges when the nuclear force is modeled with the state-of-the-art chiral effective field theory (EFT) (e.g., [9–12]). Chiral EFT starts from nucleon and pion degrees of freedom, while accounting for the symmetry and symmetry-breaking patterns of the underlying theory of quantum chromodynamics (QCD). Chiral EFT hence provides a link to quark-gluon physics, which at low energies relevant to nuclei is encapsulated in its so-called low energy constants (LECs). The nuclear force thus

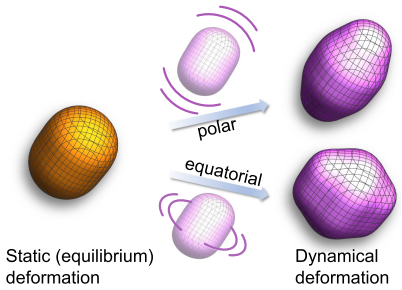

FIG. 1. Schematic illustration, based on large-scale *ab initio* calculations [1], of the static deformation (yellow) of a nuclear shape and two snapshots of its dynamical deformation (purple) arising from energetic surface oscillations (particle-hole excitations): "polar" aligned with the symmetry axis, and "equatorial" in the orthogonal plane.

partly depends on these unknown parameters which are typically fit to experimental few-nucleon data and might eventually be informed by QCD [13–15]. In this framework, we can directly probe the response of collective observables to the physics at very short distances by varying the subset of LECs that determine the nucleon-nucleon (NN) contact interaction strengths.

In this Letter, we report on a surprising new result: that nuclear collectivity can be enhanced not only through the traditional mechanism of shapes with ever-larger deformation, but also by a spatial redistribution—mediated by the short-range S-wave NN contact interaction—of the surface oscillations of a single nuclear shape. Specifically, we discover that the LEC-independent part of the interaction, which includes the long-range one-pion-exchange force, determines the shapes and their contributions within a nuclear state, while at the same time variations of the short-range forces can further increase or decrease collectivity. The unexpected origin of this interesting effect, we find here, is subtle changes in the surface oscillations of one largely deformed and predominant shape, and the corresponding competition toward lower total kinetic energy or potential energy of the nucleus.

We examine this by providing, for the first time, response analyses of nuclear quadrupole moments, presented here for low-lying states of the odd-odd and prolate ^{6}Li, and the even-even and oblate ^{12}C, while using sensitivity analyses to detect correlations or a lack thereof among the LECs. The sensitivity calculations utilize the methodology of global sensitivity analysis (GSA) [16,17], which is often prohibitively expensive since the number of model evaluations required for convergence grows rapidly with the number of model parameters. Fortunately, the symmetry-adapted no-core shell model (SA-NCSM) [18–20] alleviates the cost of each evaluation by utilizing a fraction of ultralarge no-core shell model spaces without compromising the accuracy of the results. The SA-NCSM is an *ab initio* approach that has provided successful descriptions of electric quadrupole moments [18] and transition strengths without utilizing effective charges [7,8,21], beta decays and energy spectra [22,23], clustering features [22,24,25], and even reaction dynamics [18,26–28], up through the calcium region. It produces the same results as the traditional no-core shell model [29,30] for a given internucleon interaction, characterized by the number of harmonic oscillator (HO) shells accessible to the nucleons, and the HO intershell energy $\hbar\Omega$. Within this framework, we probe the response of collective features to variations in the short-distance NN coupling strengths, given by eleven LECs in chiral two-body potentials that are associated with the contact interactions of two nucleons, shedding new light on emergent collectivity in nuclei.

Resilience of nuclear shapes—To achieve this, we start with the NNLO$_{\rm opt}$ chiral NN potential [31], which is used without three-nucleon forces shown to contribute minimally

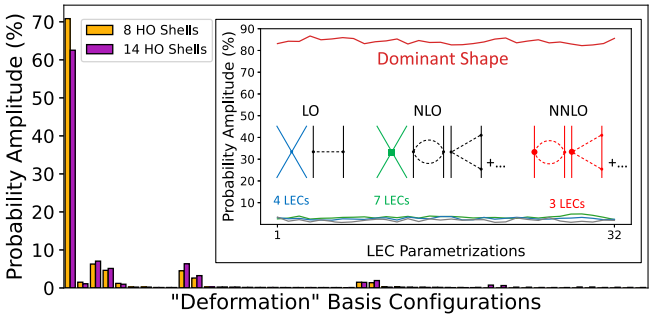

FIG. 2. Probability amplitudes of the "deformation" basis configurations of the ^{6}Li $1^{+}_{\rm g.s.}$ ground state calculated with NNLO$_{\rm opt}$ in complete model spaces of 8 (yellow) and 14 (purple) HO shells (shown are contributions with probability amplitude $\geq 0.1\%$). Inset: The four nuclear shapes with the largest probability amplitudes in the 8-shell ^{6}Li $1^{+}_{\rm g.s.}$ state across 32 NN parametrizations uniformly sampled within $\pm 10\%$ around the 14 NNLO$_{\rm opt}$ coupling constants (see text for details; cf. Supplemental Material, Fig. 1 [34] for the ^{6}Li 3^{+}_{1} state). While not shown, the inset results remain practically unchanged for 1%–50% LEC variations [42]. Also shown are the Feynman diagrams for chiral NN forces up to NNLO with the total number of LECs per order.

to three- and four-nucleon binding energies [31]. This potential is parametrized by 14 coupling constants from Feynman diagrams included up to next-to-next-to-leading order (NNLO) in the chiral expansion. Furthermore, NNLO$_{\rm opt}$ has been found to reproduce various observables and yield results equivalent to those obtained from chiral potentials that require three-nucleon forces, including, e.g., the ^{4}He electric dipole polarizability [32] and $A = 8$ energy spectra and quadrupole moments [22].

An NNLO chiral NN potential such as NNLO$_{\rm opt}$ includes the following LECs: 11 contact couplings $C^{(\rm LO)}_{^1S_0(pp,np,nn),^3S_1}$ at leading order (LO) and $C_{^1S_0,^3S_1,^3S_1-^3D_1,^3P_{0,1,2},^1P_1}$ at next-to-leading order (NLO) for a given partial wave $^{2S+1}\ell_J$, along with $c_{1,3,4}$ at NNLO which parametrize the subleading two-pion exchange interaction (Fig. 2, inset). We note that pure D-wave contact interactions are not present as they emerge at the next chiral order (N3LO), and that by using NNLO$_{\rm opt}$ this Letter adopts its regulator function and cutoff. Besides the GSA, these LECs are uniformly sampled using a Latin hypercube design [33], each bounded within $\pm 10\%$ of its NNLO$_{\rm opt}$ value.

First, using NNLO$_{\rm opt}$, we perform SA-NCSM calculations—with no *a priori* approximations or assumptions—in the so-called "deformation" many-body basis, known as the SU(3)-adapted basis [19,43]. We use complete model spaces, that is, with all possible basis states given the number of accessible HO shells. Clearly, as shown in Fig. 2 for the $1^{+}_{\rm g.s.}$ state of ^{6}Li, the probability amplitudes calculated in a model space of 8 HO shells vary only slightly compared to those calculated in the drastically

larger model space spanned by 14 HO shells. Similar outcomes are observed for excitation energies and quadrupole moments (see Fig. 4 in Supplemental Material [34]). These results indicate that the 8-shell model spaces are sufficient for our analysis that requires hundreds of thousands of large-scale computations, especially since the focus here is on responses to variations in the coupling constants and the physics that tracks with such changes. In addition, without loss of generality, our calculations use a single $\hbar\Omega = 15$ MeV, for which the rms radii converge comparatively faster (see Ref. [1], Supplemental Material [34]).

A very interesting result emerges when we further consider the ^{6}Li ground state in the so-called "shape" many-body basis, known as the physically relevant $\mathrm{Sp}(3,\mathbb{R})$-adapted basis [1,18–20]. $\mathrm{Sp}(3,\mathbb{R})$-preserving subspaces represent microscopic nuclear shapes [3,44,45], each of which includes a static deformation and its dynamical energetic surface oscillations (Fig. 1). By "energetic oscillations" we mean multiples of $2\hbar\Omega$ 1-particle-1-hole monopole and quadrupole excitations (here, multiples of 30-MeV 1-particle-1-hole excitations), different from historically used low-energy nuclear vibrations including the so-called β and γ vibrations [2]. Remarkably, as shown in the inset of Fig. 2, the shapes—and above all the dominant shape contributing 82.2%–86.6% to the $1^+_{\mathrm{g.s.}}$ state—are left practically untouched across the 10% LEC variations (see Supplemental Material Fig. 1 of [34] for all the states under consideration). This implies that the one-pion and leading two-pion exchange forces, which do not depend on the 14 LECs, determine the shapes and their contributions within a nuclear state. We note that for the $\mathrm{NNLO}_{\mathrm{opt}}$ parametrization, the most dominant shape comprises about 86% of the ^{6}Li wave functions, whereas fourteen shapes recover about 97% of the total probabilities. In a simple picture of rigid shapes that rotate, the quadrupole moment will only vary as these probabilities vary [23,45]. Given the resilience of the nuclear shapes to LEC variations, should one then expect merely marginal effects on quadrupole moments? To answer this question, we first perform GSA on the Q_2 of collective states.

Sensitivity of collective observables—Sensitivity analyses (e.g., [46,47]) are critical toward achieving higher-quality chiral potentials with rigorous uncertainty quantification (e.g., [42,48,49]), which, in turn, is key to advancing the frontier of nuclear large-scale simulations. Such studies further our understanding of dominant and exotic features of deformed nuclei, including clustering, octupole deformation, and nuclear properties that probe physics beyond the standard model (e.g., [50–52]). Here, in addition to reporting the first GSA for quadrupole moments, our main goal is slightly different, namely, we simultaneously vary all 14 parameters to demonstrate that Q_2 is mainly sensitive to changes in the couplings individually, which allows us to independently examine different parts of the interaction.

We generate 300 000 samples in the LEC parameter space using Saltelli's procedure, implemented by the Python library SALib [53,54]. With the aid of high-performance computing, these parametrizations are used for the state-of-the-art evaluation of 300 000 nuclear simulations—only possible in the shape basis—of the energy and Q_2 moment of the 3^+_1 state of ^{6}Li and of the 2^+_1 state of ^{12}C (for the ^{6}Li $1^+_{\mathrm{g.s.}}$, see Supplemental Material Fig. 2 in [34]). We find a pronounced sensitivity of Q_2 to two singlet (spin-zero) and triplet (spin-one) S-wave contacts, namely, $C_{^3S_1}^{(\mathrm{LO})}$ and $C_{^1S_0}$ (Fig. 3). This is indicated by the first-order sensitivity indices $\mathcal{S}_i$, quantifying the fractional variances in the samples due to the ith coupling alone. These are the same coupling constants to which their binding energies are most sensitive, as earlier recognized in ^{16}O [46], in contrast to the excitation energies (Fig. 3, inset). In addition, Ref. [55] has shown that the 4^+ to 2^+ energy ratio in selected neon and magnesium isotopes is most sensitive to the subleading singlet S-wave contact and a pion-nucleon coupling, with no dominant triplet S-wave feature.

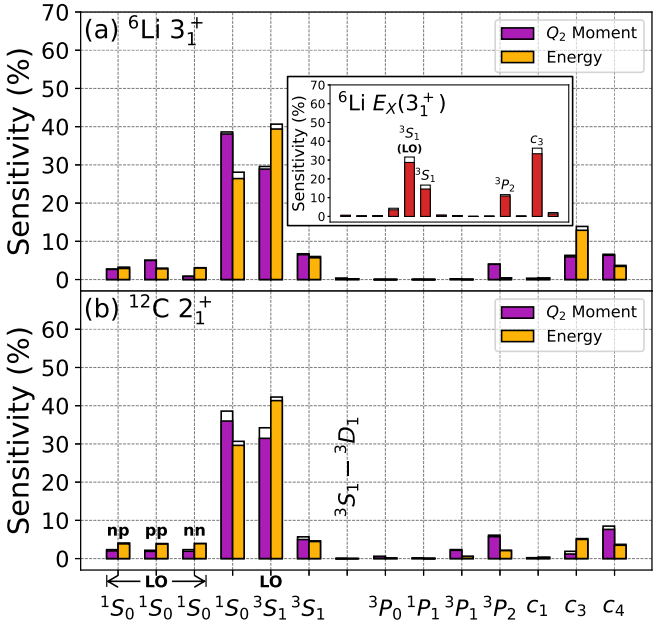

FIG. 3. First-order (colored) and total-order (white) sensitivity indices of the quadrupole moments (purple) and energies (yellow) of (a) the ^{6}Li 3^+_1 and (b) ^{12}C 2^+_1 states for each LEC. Calculations use SA model spaces comprised of fourteen shapes spanning 8 HO shells. Inset: Sensitivity indices for the ^{6}Li 3^+_1 excitation energy, $E_X(3^+)$.

To enable this huge number of calculations, required for convergence of the GSA results, we utilize symmetry-adapted (SA) model spaces selected from fourteen shapes spanning 8 HO shells. We find that the resulting sensitivity patterns are practically unchanged across various model space selections and sizes. We show this for ^{6}Li in model spaces comprised of 1 shape, 14 shapes, and all possible shapes (corresponding to the complete model space), and in larger model spaces comprised of 10 and 12 HO shells in

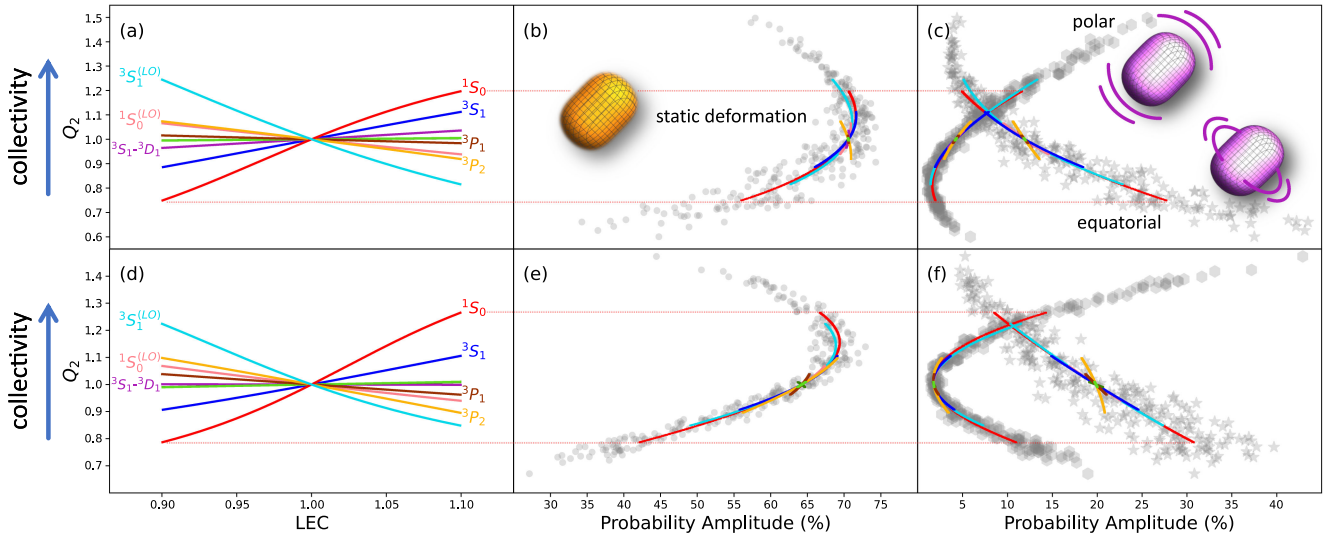

FIG. 4. Quadrupole moments Q_2 relative to their $\mathrm{NNLO_{opt}}$ values, of (a)–(c) the ^{6}Li 3_1^+ and (d)–(f) ^{12}C 2_1^+ states for each contact LEC (represented by solid curves of the same color in all plots), individually varied $\pm 10\%$ around its $\mathrm{NNLO_{opt}}$ value. For a given Q_2, or the corresponding LEC (see the dotted lines for $^1S_0$ as an example), the dominant shape is decomposed into static (0p-0h) deformation in (b) and (e), and polar (equatorial) surface oscillations along (perpendicular to) the symmetry axis in (c) and (f), shown by their probability amplitudes. Q_2 moments obtained from 300 samples of the 14 LECs varied simultaneously are shown in gray for the static (circles), polar (hexagons), and equatorial deformation (stars). In all plots for ^{6}Li, the model space is expanded to 12 HO shells.

Supplemental Material Figs. 2 and 3 of [34], respectively. Using the same shape-selection prescription [43] and a different set of fourteen shapes, the sensitivity analysis becomes feasible for the ^{12}C 2_1^+ state. In this way, one can utilize Hamiltonian matrices in the selected shape basis of highly reduced dimensions (e.g., four orders of magnitude reduction for the 2_1^+) that can serve as emulators, similarly to, e.g., [56–62]. Indeed, we find that the sensitivity pattern for ^{12}C [Fig. 3(b)] closely resembles that of ^{6}Li.

Importantly, the total-order sensitivity indices, which additionally include correlations with all remaining LECs, practically coincide with the first-order indices $\mathcal{S}_i$ (Fig. 3). This suggests that the main effect of each coupling constant on Q_2 is largely decoupled from those of the remaining parameters, and can be explored separately. This is especially useful since the sensitivity indices are normalized to the total variance of the Q_2 distributions sampled, and thus provide a relative contribution to the variance, regardless whether the variance itself is small or large. The way in which each contact coupling affects the magnitude of Q_2 itself can hence be understood by studying the responses of the LECs individually, as discussed next.

Short-range footprints on long-range physics—We find that non-negligible nuclear quadrupole moments of collective states, such as the ^{6}Li 3_1^+ and ^{12}C 2_1^+ states, can be enhanced by nearly 40% through the simultaneous action of two competing S-wave contact interactions, which do so via an unexpected mechanism. To show this, we first fix all coupling constants but one to their $\mathrm{NNLO_{opt}}$ values, and draw 300 samples for each individual LEC, following a Latin hypercube design (Fig. 4, where for visual clarity we exclude the LO proton-proton and neutron-neutron $^1S_0$ contacts, and since we focus on the contact physics, similarly exclude c_1, c_3, and c_4; for completeness, we provide all these in [34]).

Corroborating the GSA results of Fig. 3 and Supplemental Material Fig. 2 [34], Fig. 4 unveils additionally interesting features, namely, that Q_2 depends practically linearly on the LECs, and that the S-wave contacts act in opposition: increasing the LO S-wave couplings (especially the triplet $^3S_1$) of the attractive delta contact interaction decreases Q_2, while increasing the coupling strength of the repulsive NLO S-wave contact (dominated by the singlet $^1S_0$) results in larger Q_2 moments. We note that the stronger the LO $^3S_1$ coupling, the more bound the deuteron system is, and that an attractive delta interaction has historically been used to describe pairing. Indeed, in phenomenological nuclear models, increasing the pairing strength leads to some decrease in Q_2 through the mixing of nuclear shapes [63]. Surprisingly, Fig. 4 shows such a decrease in Q_2, but with practically no change in the mixing of the nuclear shapes, as discussed above (see Supplemental Material Fig. 1 [34]; cf. Fig. 2). This suggests that another mechanism might be responsible. Given the large probability amplitudes of the dominant nuclear shapes, we explore whether the observed variances of Q_2 are tied to changes within these dominant shapes. Importantly, since the total quadrupole moment is the sum of Q_2 contributions from each nuclear shape (as Q_2 does not couple different shapes), the component of Q_2 attributed to the dominant shape not only yields

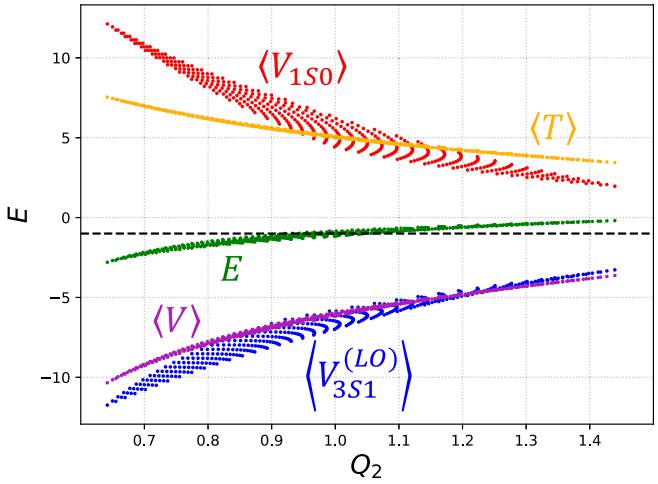

FIG. 5. The total energy $E = \langle T + V \rangle$ of the ^{6}Li 3_1^+ state (green), the expectation value of the total potential energy $\langle V \rangle$ (purple) and total kinetic energy $\langle T \rangle$ (yellow), as well as of the LO $^3S_1$ and NLO $^1S_0$ potentials (blue and red, respectively), as functions of the electric quadrupole moment Q_2. The quadrupole moments are normalized to their NNLO$_{\rm opt}$ values; the expectation values are all normalized to the absolute value of the NNLO$_{\rm opt}$ 3_1^+ energy. Increasing Q_2 values correspond to increases (decreases) in the strength of the subleading $^1S_0$ (leading $^3S_1$) LEC (Supplemental Material Fig. 6 in [34]).

most of the total Q_2 value, but also exhibits nearly identical LEC dependence [e.g., for the $1_{\rm g.s.}^+$, see Fig. 7(a) in the Supplemental Material [34], dashed lines].

The physics of the dominant shape unveils, for the first time, the unexpected result that the S-wave contacts of the underlying chiral potential can significantly alter the magnitude of Q_2 by impacting the shape's surface dynamics: the magnitude of Q_2 increases for a stronger repulsive $^1S_0$ contact interaction by favoring polar oscillations, that is, multiples of two HO quanta along the symmetry axis, and decreases as the equatorial modes (having HO quanta in the plane perpendicular to the symmetry axis) become dominant with a more attractive $^3S_1$ contact [Figs. 4(c) and 4(f)]. This can be understood as follows: the repulsive $^1S_0$ contact, by spreading nucleons to higher HO shells, reduces Pauli-principle constraints and makes prolate configurations accessible, and these are known to have low kinetic energy [64,65], as illustrated in Fig. 5. In contrast to this, as the leading $^3S_1$ coupling of the attractive delta contact increases, excitations in the equatorial plane become favorable, leading to a further decrease of the negative potential energy (Fig. 5); and while this results in larger binding energy, it comes at the expense of reduced collectivity.

These two contacts together, when varied by only 10% each, can impact Q_2 by up to ∼40% for the ^{6}Li 3_1^+ and ^{12}C 2_1^+ collective states (see Fig. 5 for the 3_1^+ state). This is also larger compared to ∼6%–13% many-body model uncertainties (see, e.g., Fig. 4 of Supplemental Material [34] and Refs. [66,67] for the infinite-space estimates for Q_2 using NNLO$_{\rm opt}$ for ^{6}Li and ^{12}C). Furthermore, the importance of the polar modes cannot be understated: whether the equilibrium deformation is prolate as in ^{6}Li, or oblate as in ^{12}C, only polar oscillations will enhance collectivity. In short, we link the impact of the short-distance contact physics on nuclear collectivity to the surface dynamics that can increase (decrease) Q_2 predominantly through a stronger repulsive NLO (attractive LO) S-wave contact that favors polar (equatorial) oscillations, which lower the kinetic (potential) energy. This impact is not merely marginal, which in turn makes quadrupole moments important observables to constrain realistic nuclear forces. Furthermore, we find similar outcomes when varying the LECs of another chiral potential (NNLO$_{\rm sat}$ [68]), and for the intermediate-mass triaxial nucleus of ^{22}Mg (Fig. 5 of Supplemental Material [34]).

To summarize, we find that electric quadrupole moments of light deformed nuclei, which provide a measure of their collectivity, are affected up to about 40% when two short-range chiral NN interactions are simultaneously varied within a comparatively smaller 10% range, specifically, the opposing attractive triplet and repulsive singlet S-wave contacts. Most importantly, while historically larger Q_2 moments have been associated with reduced mixing between nuclear shapes or shapes of larger deformation, here, for the first time, we show that contact interactions can significantly increase the magnitude of Q_2 by subtly altering the surface dynamics of (typically) one dominant nuclear shape. We show that quadrupole collectivity is maximized by enhancing the polar surface oscillations, and this is most readily accomplished by increasing the magnitude of the subleading $^1S_0$ coupling or decreasing that of the leading $^3S_1$ contact, both of which lower the total kinetic energy. We have thus found a direct link between an *ab initio* description of nuclear collectivity and the short-range part of the underlying strong forces between two nucleons in contact, modeled in the chiral EFT framework, shedding new light on the emergent collectivity that dominates nuclear dynamics.

Acknowledgments—This work was supported by the U.S. Department of Energy (No. DE-SC0023532), and in part by the National Nuclear Security Administration through the Center for Excellence in Nuclear Training and University Based Research (CENTAUR) under Grant No. DE-NA-0004150, the European Research Council (ERC) under the European Union's Horizon 2020 research and innovation program (Grant Agreement No. 758027), the Swedish Research Council (Grant Agreements No. 2020-05127 and No. 2024-04681), and the Czech Science Foundation (No. 22-14497S). This material is based upon work supported by the U.S. Department of Energy, Office of Science, Office of Nuclear Physics, under

the FRIB Theory Alliance Award No. DE-SC0013617. This work benefited from high performance computational resources provided by LSU, the National Energy Research Scientific Computing Center (NERSC), a U.S. Department of Energy Office of Science User Facility at Lawrence Berkeley National Laboratory operated under Contract No. DE-AC02-05CH11231, as well as the Frontera computing project at the Texas Advanced Computing Center, made possible by National Science Foundation Grant No. OAC-1818253.

Data availability—The data that support the findings of this article are not publicly available upon publication because it is not technically feasible and/or the cost of preparing, depositing, and hosting the data would be prohibitive within the terms of this research project. The data are available from the authors upon reasonable request.

[1] T. Dytrych, K. D. Launey, J. P. Draayer, D. J. Rowe, J. L. Wood, G. Rosensteel, C. Bahri, D. Langr, and R. B. Baker, Physics of nuclei: Key role of an emergent symmetry, Phys. Rev. Lett. **124**, 042501 (2020).

[2] A. Bohr and B. R. Mottelson, *Nuclear Structure* (Benjamin, New York, 1969), Vol. 1.

[3] D. J. Rowe, The emergence and use of symmetry in the many-nucleon model of atomic nuclei, in *Emergent Phenomena in Atomic Nuclei from Large-Scale Modeling: A Symmetry-Guided Perspective* (World Scientific Publishing Co., Singapore, 2017), p. 65.

[4] K. Heyde and J. L. Wood, Shape coexistence in atomic nuclei, Rev. Mod. Phys. **83**, 1467 (2011).

[5] P. E. Garrett, M. Zielińska, and E. Clément, An experimental view on shape coexistence in nuclei, Prog. Part. Nucl. Phys. **124**, 103931 (2022).

[6] A. E. Stuchbery and J. L. Wood, To shell model, or not to shell model, that is the question, MDPI Phys. **4**, 697 (2022).

[7] J. Henderson *et al.*, Testing microscopically derived descriptions of nuclear collectivity: Coulomb excitation of ^{22}Mg, Phys. Lett. B **782**, 468 (2018).

[8] P. Ruotsalainen *et al.*, Isospin symmetry in $B(E2)$ values: Coulomb excitation study of ^{21}Mg, Phys. Rev. C **99**, 051301 (R) (2019).

[9] P. F. Bedaque and U. van Kolck, Effective field theory for few-nucleon systems, Annu. Rev. Nucl. Part. Sci. **52**, 339 (2002).

[10] D. R. Entem and R. Machleidt, Accurate charge-dependent nucleon-nucleon potential at fourth order of chiral perturbation theory, Phys. Rev. C **68**, 041001(R) (2003).

[11] E. Epelbaum, H. Krebs, and U.-G. Meißner, Precision nucleon-nucleon potential at fifth order in the chiral expansion, Phys. Rev. Lett. **115**, 122301 (2015).

[12] H.-W. Hammer, S. König, and U. van Kolck, Nuclear effective field theory: Status and perspectives, Rev. Mod. Phys. **92**, 025004 (2020).

[13] R. A. Briceño, Z. Davoudi, T. C. Luu, and M. J. Savage, Two-nucleon systems in a finite volume. II. $^3S_1 - {}^3D_1$ coupled channels and the deuteron, Phys. Rev. D **88**, 114507 (2013).

[14] C. McIlroy, C. Barbieri, T. Inoue, T. Doi, and T. Hatsuda, Doubly magic nuclei from lattice QCD forces at $M_{\rm PS} = 469$ MeV$/c^2$, Phys. Rev. C **97**, 021303(R) (2018).

[15] I. Tews, Z. Davoudi, A. Ekström, J. D. Holt, and J. E. Lynn, New ideas in constraining nuclear forces, J. Phys. G **47**, 103001 (2020).

[16] I. M. Sobol', Global sensitivity indices for nonlinear mathematical models and their Monte Carlo estimates, Math. Comput. Simul. **55**, 271 (2001).

[17] A. Saltelli, P. Annoni, I. Azzini, F. Campolongo, M. Ratto, and S. Tarantola, Variance based sensitivity analysis of model output. Design and estimator for the total sensitivity index, Comput. Phys. Commun. **181**, 259 (2010).

[18] K. D. Launey, A. Mercenne, and T. Dytrych, Nuclear dynamics and reactions in the *ab initio* symmetry-adapted framework, Annu. Rev. Nucl. Part. Sci. **71**, 253 (2021).

[19] K. D. Launey, T. Dytrych, and J. P. Draayer, Symmetry-guided large-scale shell-model theory, Prog. Part. Nucl. Phys. **89**, 101 (review) (2016).

[20] T. Dytrych, K. D. Sviratcheva, C. Bahri, J. P. Draayer, and J. P. Vary, Evidence for symplectic symmetry in *ab initio* no-core shell model results for light nuclei, Phys. Rev. Lett. **98**, 162503 (2007).

[21] J. Williams *et al.*, Structure of ^{28}Mg and influence of the neutron pf shell, Phys. Rev. C **100**, 014322 (2019).

[22] G. H. Sargsyan, K. D. Launey, M. T. Burkey, A. T. Gallant, N. D. Scielzo, G. Savard, A. Mercenne, T. Dytrych, D. Langr, L. Varriano, B. Longfellow, T. Y. Hirsh, and J. P. Draayer, Impact of clustering on the ^{8}Li β decay and recoil form factors, Phys. Rev. Lett. **128**, 202503 (2022).

[23] N. D. Heller, G. H. Sargsyan, K. D. Launey, C. W. Johnson, T. Dytrych, and J. P. Draayer, New insights into backbending in the symmetry-adapted shell-model framework, Phys. Rev. C **108**, 024304 (2023).

[24] A. C. Dreyfuss, K. D. Launey, J. E. Escher, G. H. Sargsyan, R. B. Baker, T. Dytrych, and J. P. Draayer, Clustering and α-capture reaction rate from *ab initio* symmetry-adapted descriptions of ^{20}Ne, Phys. Rev. C **102**, 044608 (2020).

[25] A. C. Dreyfuss, K. D. Launey, T. Dytrych, J. P. Draayer, R. B. Baker, C. M. Deibel, and C. Bahri, Understanding emergent collectivity and clustering in nuclei from a symmetry-based no-core shell-model perspective, Phys. Rev. C **95**, 044312 (2017).

[26] A. Mercenne, K. D. Launey, J. E. Escher, T. Dytrych, and J. P. Draayer, New *ab initio* approach to nuclear reactions based on the symmetry-adapted no-core shell model, in *Recent Progress in Few-Body Physics*, edited by N. Orr, M. Ploszajczak, F. Marques, and J. Carbonell, Springer Proceedings in Physics Vol. 238 (Springer, Cham, 2020), p. 253, 10.1007/978-3-030-32357-8_44.

[27] A. Mercenne, K. D. Launey, T. Dytrych, J. E. Escher, S. Quaglioni, G. H. Sargsyan, D. Langr, and J. P. Draayer, Efficacy of the symmetry-adapted basis for *ab initio* nucleon-nucleus interactions for light- and intermediate-mass nuclei, Comput. Phys. Commun. **280**, 108476 (2022).

[28] M. Burrows, R. B. Baker, S. Bacca, K. D. Launey, T. Dytrych, and D. Langr, Response functions and giant monopole resonances for light to medium-mass nuclei from

the *ab initio* symmetry-adapted no-core shell model, J. Phys. G **52**, 035107 (2025).
[29] P. Navrátil, J. P. Vary, and B. R. Barrett, Properties of ^{12}C in the *ab initio* nuclear shell model, Phys. Rev. Lett. **84**, 5728 (2000).
[30] B. R. Barrett, P. Navrátil, and J. P. Vary, *Ab initio* no core shell model, Prog. Part. Nucl. Phys. **69**, 131 (2013).
[31] A. Ekström, G. Baardsen, C. Forssén, G. Hagen, M. Hjorth-Jensen, G. R. Jansen, R. Machleidt, W. Nazarewicz, T. Papenbrock, J. Sarich, and S. M. Wild, Optimized chiral nucleon-nucleon interaction at next-to-next-to-leading order, Phys. Rev. Lett. **110**, 192502 (2013).
[32] R. B. Baker, K. D. Launey, S. Bacca, N. N. Dinur, and T. Dytrych, Benchmark calculations of electromagnetic sum rules with a symmetry-adapted basis and hyperspherical harmonics, Phys. Rev. C **102**, 014320 (2020).
[33] M. D. Mckay, R. J. Beckman, and W. J. Conover, A comparison of three methods for selecting values of input variables in the analysis of output from a computer code, Technometrics **42**, 55 (2000).
[34] See Supplemental Material at http://link.aps.org/supplemental/10.1103/c3st-tp13 for the model convergence of the presented calculations and further technical details for the methods used, which includes Refs. [35–41].
[35] A. Saltelli, Making best use of model evaluations to compute sensitivity indices, Comput. Phys. Commun. **145**, 280 (2002).
[36] T. Homma and A. Saltelli, Importance measures in global sensitivity analysis of nonlinear models, Reliab. Eng. Syst. Safety **52**, 1 (1996).
[37] B. J. Verhaar, A method for the elimination of spurious states in the nuclear harmonic oscillator shell model, Nucl. Phys. **21**, 508 (1960).
[38] K. T. Hecht, The use of SU(3) in the elimination of spurious center of mass states, Nucl. Phys. **A170**, 34 (1971).
[39] T. Dytrych, K. D. Launey, J. P. Draayer, P. Maris, J. P. Vary, E. Saule, U. Catalyurek, M. Sosonkina, D. Langr, and M. A. Caprio, Collective modes in light nuclei from first principles, Phys. Rev. Lett. **111**, 252501 (2013).
[40] P. Maris, J. P. Vary, and P. Navrátil, Structure of $A = 7$–8 nuclei with two- plus three-nucleon interactions from chiral effective field theory, Phys. Rev. C **87**, 014327 (2013).
[41] K. D. Launey, T. Dytrych, and J. P. Draayer, Similarity renormalization group and many-body effects in multiparticle systems, Phys. Rev. C **85**, 044003 (2012).
[42] K. S. Becker, K. D. Launey, A. Ekström, T. Dytrych, D. Langr, G. H. Sargsyan, and J. P. Draayer, Uncertainty quantification of collective nuclear observables from the chiral potential parametrization, Phys. Scr. **99**, 125311 (2024).
[43] K. D. Launey, T. Dytrych, G. H. Sargsyan, R. B. Baker, and J. P. Draayer, Emergent symplectic symmetry in atomic nuclei: *Ab initio* symmetry-adapted no-core shell model, Eur. Phys. J. Special Topics **229**, 2429 (2020).
[44] G. Rosensteel and D. J. Rowe, Nuclear $\mathrm{Sp}(3, R)$ model, Phys. Rev. Lett. **38**, 10 (1977).
[45] D. J. Rowe, Microscopic theory of the nuclear collective model, Rep. Prog. Phys. **48**, 1419 (1985).
[46] A. Ekström and G. Hagen, Global sensitivity analysis of bulk properties of an atomic nucleus, Phys. Rev. Lett. **123**, 252501 (2019).
[47] A. Belley, J. Pitcher, T. Miyagi, S. R. Stroberg, and J. D. Holt, Correlation of neutrinoless double-beta decay nuclear matrix elements with nucleon-nucleon phase shifts, arXiv:2408.02169.
[48] B. D. Carlsson, A. Ekström, C. Forssén, D. F. Strömberg, G. R. Jansen, O. Lilja, M. Lindby, B. A. Mattsson, and K. A. Wendt, Uncertainty analysis and order-by-order optimization of chiral nuclear interactions, Phys. Rev. X **6**, 011019 (2016).
[49] I. Svensson, A. Ekström, and C. Forssén, Bayesian estimation of the low-energy constants up to fourth order in the nucleon-nucleon sector of chiral effective field theory, Phys. Rev. C **107**, 014001 (2023).
[50] S. Shen, S. Elhatisari, T. A. Lähde, D. Lee, B.-N. Lu, and U.-G. Meißner, Emergent geometry and duality in the carbon nucleus, Nat. Commun. **14**, 2777 (2023).
[51] M. Frosini, T. Duguet, J.-P. Ebran, B. Bally, T. Mongelli, T. R. Rodríguez, R. Roth, and V. Somà, II. *Ab initio* study of neon isotopes via PGCM and IM-NCSM calculations, Eur. Phys. J. A **58**, 63 (2022).
[52] J. M. Yao, B. Bally, J. Engel, R. Wirth, T. R. Rodríguez, and H. Hergert, *Ab initio* treatment of collective correlations and the neutrinoless double beta decay of ^{48}Ca, Phys. Rev. Lett. **124**, 232501 (2020).
[53] J. Herman and W. Usher, SALib: An open-source Python library for sensitivity analysis, J. Open Source Software **2**. 97 (2017).
[54] T. Iwanaga, W. Usher, and J. Herman, Toward SALib 2.0: Advancing the accessibility and interpretability of global sensitivity analyses, SESMO **4**, 18155 (2022).
[55] Z. H. Sun, A. Ekström, C. Forssén, G. Hagen, G. R. Jansen, and T. Papenbrock, Multiscale physics of atomic nuclei from first principles, Phys. Rev. X **15**, 011028 (2025).
[56] D. Frame, R. He, I. Ipsen, D. Lee, D. Lee, and E. Rrapaj, Eigenvector continuation with subspace learning, Phys. Rev. Lett. **121**, 032501 (2018).
[57] S. König, A. Ekström, K. Hebeler, D. Lee, and A. Schwenk, Eigenvector continuation as an efficient and accurate emulator for uncertainty quantification, Phys. Lett. B **810**, 135814 (2020).
[58] T. Djärv, A. Ekström, C. Forssén, and H. T. Johansson, Bayesian predictions for $A = 6$ nuclei using eigenvector continuation emulators, Phys. Rev. C **105**, 014005 (2022).
[59] K. S. Becker, K. D. Launey, A. Ekström, and T. Dytrych, *Ab initio* symmetry-adapted emulator for studying emergent collectivity and clustering in nuclei, Front. Phys. **11**, 1064601 (2023).
[60] D. Odell, P. Giuliani, K. Beyer, M. Catacora-Rios, M. Y.-H. Chan, E. Bonilla, R. J. Furnstahl, K. Godbey, and F. M. Nunes, ROSE: A reduced-order scattering emulator for optical models, Phys. Rev. C **109**, 044612 (2024).
[61] T. Duguet, A. Ekström, R. J. Furnstahl, S. König, and D. Lee, Colloquium: Eigenvector continuation and projection-based emulators, Rev. Mod. Phys. **96**, 031002 (2024).
[62] N. Yapa, S. König, and K. Fossez, Toward scalable bound-to-resonance extrapolations for few- and many-body systems, Phys. Rev. C **111**, 064318 (2025).
[63] J. E. Escher, C. Bahri, D. Troltenier, and J. P. Draayer, Pairing-plus-quadrupole model and nuclear deformation:

A look at the spin-orbit interaction, Nucl. Phys. **A633**, 662 (1998).

[64] B. Castel, D. J. Rowe, and L. Zamick, Why are deformed nuclei prolate?, Phys. Lett. B **236**, 121 (1990).

[65] D. J. Rowe, How do deformed nuclei rotate?, Nucl. Phys. **A152**, 273 (1970).

[66] I. J. Shin, Y. Kim, P. Maris, J. P. Vary, C. Forssén, J. Rotureau, and N. Michel, *Ab initio* no-core solutions for ^{6}Li, J. Phys. G **44**, 075103 (2017).

[67] G. H. Sargsyan, Electromagnetic transitions and beta decays in nuclei from the *ab initio* symmetry-adapted no-core shell model, Ph. D. thesis, Louisiana State University (2021), LSU Doctoral Dissertations, p. 5641, https://repository.lsu.edu/gradschool_dissertations/5641.

[68] A. Ekström, G. R. Jansen, K. A. Wendt, G. Hagen, T. Papenbrock, B. D. Carlsson, C. Forssén, M. Hjorth-Jensen, P. Navrátil, and W. Nazarewicz, Accurate nuclear radii and binding energies from a chiral interaction, Phys. Rev. C **91**, 051301(R) (2015).